Proceedings of the Institution of Mechanical Engineers, Part C: Journal of Mechanical Engineering Science
http://pic.sagepub.com/

Regular and chaotic dynamics of a simplified fly-ball governor

Z-M Ge, C-S Chen, H-H Chen and S-C Lee

Proceedings of the Institution of Mechanical Engineers, Part C: Journal of Mechanical Engineering Science 1999 213: 461
DOI: 10.1243/0954406991522707

Regular and chaotic dynamics of a simplified fly-ball governor

Z-M Ge*, **C-S Chen**, **H-H Chen** and **S-C Lee**
Department of Mechanical Engineering, National Chiao Tung University, Taiwan

Abstract: The dynamics of a simplified model of a fly-ball speed governor undergoing a harmonic variation about its rotational speed is studied in this paper. This system is a non-linear damped system subjected to parametric excitation. The harmonic balance method is applied to analyse the stability of period attractors and the behaviour of bifurcations. The time evolutions of the response of the non-linear dynamic system are described by time history, phase portraits and Poincaré maps. The regular and chaotic behaviour is observed by various numerical techniques such as power spectra, Lyapunov exponents and Lyapunov dimension. Finally, the domains of attraction of periodic and stranger attractors of the system are located by applying the interpolated cell mapping (ICM) method.

Keywords: governor, bifurcation, chaos, parametric excitation, cell mapping

NOTATION

A	matrix $\begin{bmatrix} 0 & 1 \\ A_{21} & -2\alpha/\omega \end{bmatrix}$
$\mathbf{B}_k$	$(1/\Delta_k)\int_{\tau_{k-1}}^{\tau_k} \mathbf{A}(\xi)\,\mathrm{d}\xi$
c	damping coefficient in the rod bearing
C	matrix $\begin{bmatrix} [C_1]_{ij} & [C_{12}]_{ij} \\ [C_{21}]_{ij} & [C_2]_{ij} \end{bmatrix}$ (in Appendix)
f	Ω_0^2
F	$-(2\omega_0\ddot{x}_0 + 2\alpha\dot{x})$
g	acceleration of gravity
L	Lagrangian
m	total mass of the fly-ball
M	mass of the collar
P	$-\sin x_0$
Q	$(1-\cos\tau)\sin 2x_0$
R	length of the rod
V	Lyapunov function
w	rotational speed of the fly-ball
x	defined as θ
X	matrix $[\delta x, \delta\dot{x}]^{\mathrm{T}}$
α	$c/(2m)$
β	mass ratio
γ	g/R
$\bar{\varepsilon}$	perturbed coefficient of the rotational speed
θ	angle between rod and vertical line
λ	Lyapunov exponent
ξ	variable of integration in equation (20)
τ	dimensionless time
$\mathbf{\Phi}$	approximate transition matrix
ω	perturbed frequency of the rotational speed
Ω_0	constant rotational speed of the fly-ball

The MS was received on 2 May 1997 and was accepted after revision for publication on 30 July 1998.
* *Corresponding author: Department of Mechanical Engineering, National Chiao Tung University, 1001 Ta Hsueh Road, Hsinchu 30050, Taiwan, Republic of China.*

1 INTRODUCTION

The dynamics of a one degree-of-freedom simplified model of a fly-ball speed governor undergoing a harmonic variation about its rotational speed is studied. Many studies have been carried out in recent years on one degree-of-freedom non-linear systems under sinusoidal forcing and a substantial understanding of the complicated phenomena that can arise from these apparently simple oscillators has been reached. The behaviour of parametrically excited systems is very complicated even when only the linear case is considered. In recent decades a number of studies on the chaotic behaviour of a parametrically excited system have been carried out by numerical techniques such as phase portraits, Poincaré maps, power spectrum and Lyapunov exponents [**1**–**3**].

Harmonic balance (HB) methods [**6**–**9**] are suited to strongly non-linear systems. Ling and Wu [**8**] have developed the fast Galerkin (FG) method which provides an efficient and accurate basis for the analysis of non-linear systems. Lau *et al.* [**9**] developed the incremental harmonic balance (IHB) method which also deals with strong non-linearities. In the IHB method the incrementation is followed by a Galerkin approximation. These methods are applied to parametric studies for the purpose of seeking parameter diagrams by changing the system parameters in turn. The multivariable Floquet theory [**6**, **7**] is applied to analyse the stability of periodic solutions through the module of eigenvalues of the associated monodromy matrix of the system.

It is well known that different initial conditions may lead to different attractors in a non-linear system. Often, stable and unstable attractors are coexistent. The attractors and corresponding basins of attraction of a non-linear system can be located by the method of interpolated cell mapping [**9**, **10**], which has been demonstrated over the past few years to high advantage in exploring global non-linear behaviour. The domains of attraction of the period and chaotic attractor with respect to initial conditions are investigated by interpolated cell mapping techniques in this paper.

2 FLY-BALL GOVERNOR WITH A SIMPLE MODEL

2.1 Mathematical model

The fly-ball speed governor (Watt governor) is shown in Fig. 1. For simplicity, it is assumed for the system that:

1. The masses of the collar and of the rods are neglected.
2. Viscous damping in the rod bearing of the fly-ball is presented by damping constant c.

The Lagrange equation is derived as follows:

$$\ddot{\theta} + \frac{c}{m}\dot{\theta} + \frac{g}{R}\sin\theta = \frac{w^2}{2}\sin 2\theta \tag{1}$$

In most cases the governor is required to rotate at constant speed and the governing device should therefore

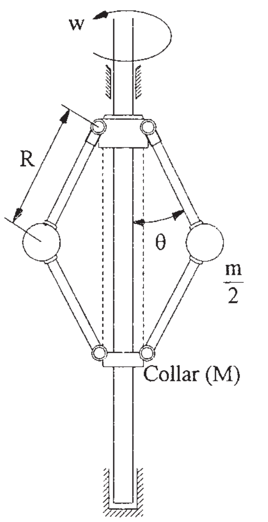

Fig. 1 Physical model of a fly-ball governor system

govern 'isochronously'. However, the speed will undergo a variation when the load of the engine changes; hence the governor must change speed with variation in load. It is assumed that the fly-ball governor rotates at constant speed and undergoes a variation with a harmonic term, i.e. $w = \Omega_0 - \bar{\varepsilon}\Omega_0 \cos\omega t$, and then (1) becomes

$$\ddot{\theta} + 2\alpha\dot{\theta} + \gamma = \frac{f}{2}\sin 2\theta - \bar{\varepsilon} f \cos\omega t \sin 2\theta + O(\bar{\varepsilon}^2) \tag{2}$$

where $2\alpha = c/m$, $\gamma = g/R$, $f = \Omega_0^2$. For simplicity, the $\bar{\varepsilon}^2$ term is neglected, $x = \theta$ is defined and equation (2) becomes

$$\ddot{x} + 2\alpha\dot{x} + \gamma \sin x = \frac{f}{2}\sin 2x - \bar{\varepsilon} f \cos\omega t \sin 2x \tag{3}$$

Obviously, equation (3) is a non-linear, one degree-of-freedom, parametrically excited system.

2.2 Lyapunov exponents and Lyapunov dimension

The Lyapunov exponents for the system under consideration can be obtained numerically. The algorithm for calculation of the Lyapunov exponents has been described in detail by Wolf *et al.* [**11**].

Parametrically excited dynamic system (3) with the chosen parameters

$$\ddot{x} + 1.4\dot{x} + 4\sin x = \frac{f}{2}(1 - \cos 8t)\sin 2x \qquad (\bar{\varepsilon} = 0.5) \tag{4}$$

possesses three Lyapunov exponents. Figures 2a and b indicate the Lyapunov exponents of the system under various parameters to determine the occurrence of chaotic motion. From Fig. 2a the exponents are

$$\lambda_1 = -0.1663, \qquad \lambda_2 = 0, \qquad \lambda_3 = -1.2337$$

and from Fig. 2b the exponents are

$$\lambda_1 = 0.7035, \qquad \lambda_2 = 0, \qquad \lambda_3 = -2.1035$$

In this linear damping case the sum of all three Lyapunov exponents is equivalent to the negative damping coefficient in the system, which is independent of the initial conditions and time [**12**]. Thus, the sum of the three Lyapunov exponents for these two cases is always -1.4. The largest Lyapunov exponent is plotted in Fig. 3 with f ranging from 0 to 30. It is clear that, when f is small, λ_1 is negative and the system is periodic. Furthermore, the values of the exponents approach zero as the solutions change their types. When f is increased to 20.76, λ_1 changes from negative to positive values; this is the critical point for the onset of chaotic motion. It is noted that in some intervals of large f, for example $f = 22.12$, the exponent becomes negative again and the system is then periodic (see Table 1, where d_f is the Lyapunov fractal dimension).

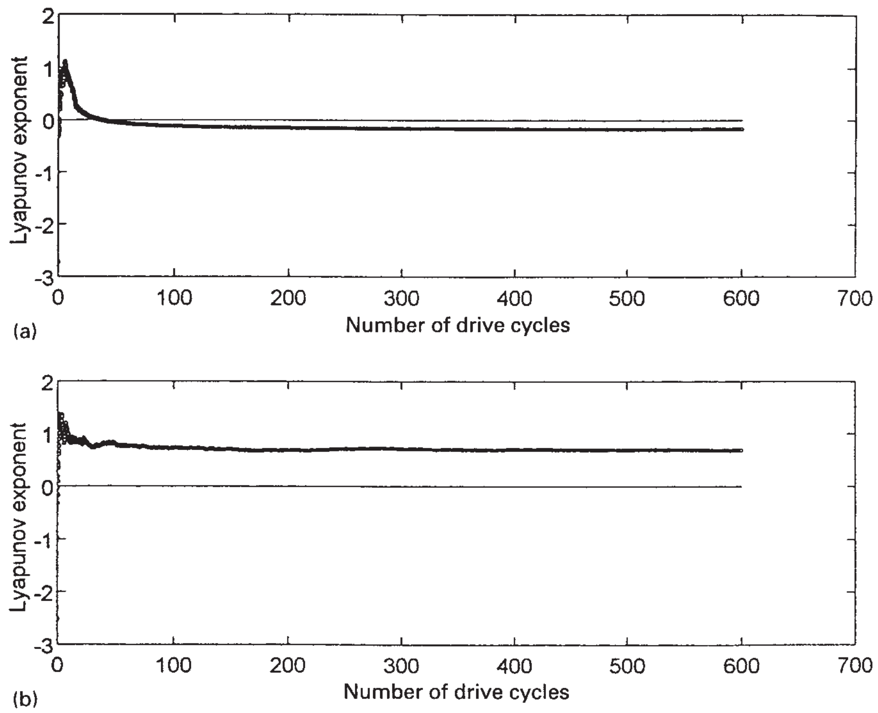

Fig. 2 Lyapunov exponents as a function of the number of drive cycles for (a) $f = 19$ and (b) $f = 23$

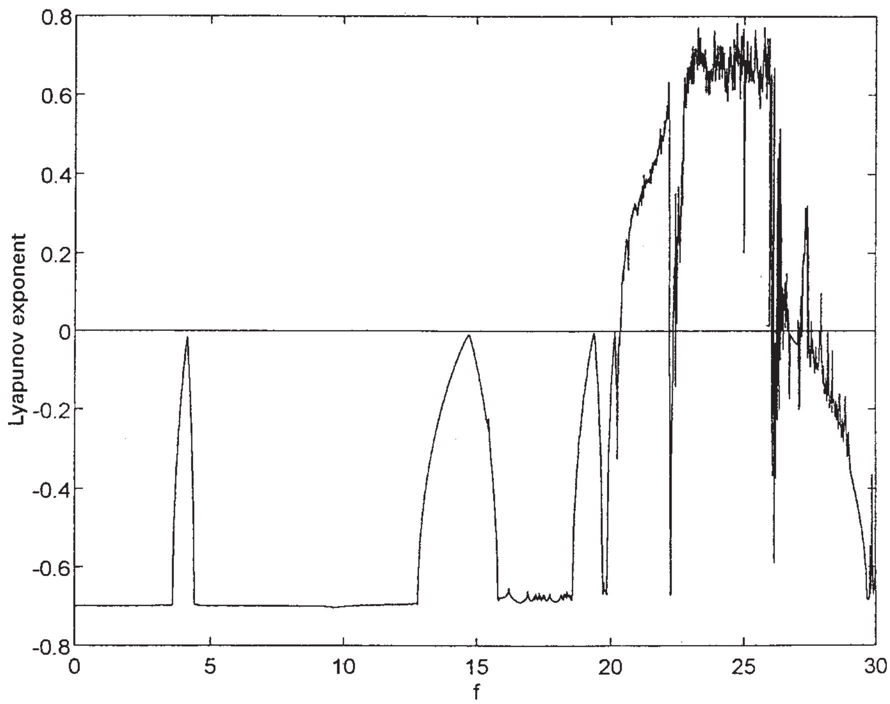

Fig. 3 Largest Lyapunov exponent as a function of f

2.3 Poincaré map, phase portraits, time history and power spectrum analysis

For each initial condition, differential equation (4) is solved by the fourth-order Runge–Kutta numerical integration method. The results obtained by Poincaré maps in comparison with phase trajectories are shown in Figs 4a to f. Note that a pair of period $2T$ motions arise and invert each other from these figures. One of the orbits that the trajectories are attracted to depends on where the initial conditions are located. When $f = 19$ the phase portraits and Poincaré maps show that the system is period $2T$ motion. When $f = 20.2$ the system is period $8T$ motion, with eight Poincaré points. It can be

Table 1 Lyapunov exponents and Lyapunov dimension for different values of f in equation (4)

	f				
	14	19	19.5	20.3	25
λ_1	-0.1212	-0.1678	-0.1297	-0.0246	0.69
λ	-1.2788	-1.2322	-1.2703	-1.3753	-2.09
$\sum_i \lambda_i$	-1.4	-1.4	-1.4	-1.4	-1.4
d_f	1	1	1	1	2.33
	Period T	Period $2T$	Period $4T$	Period $8T$	Chaotic

seen that with $f = 20.37$ and $f = 23$ the steady state Poincaré orbits of chaotic systems are distinctive. The strange attractors for $f = 20.37$ have two inverse chaotic attractors, but these two independent attractors are destroyed when $f = 23$.

The time history and power spectrum analysed for $f = 19$, 20 and 23 are shown in Figs 5a to f. It is clear that the spectrum of a periodic motion consists only of discrete frequencies, whereas the spectrum of a chaotic motion is not composed solely of discrete frequencies but has a continuous, broad band nature. This noise-like spectrum is characteristic of chaotic systems. From Fig. 5b it can be observed that a strong peak occurs at the fundamental frequency together with superharmonic frequencies. The presence of the spectral line at half the fundamental frequency shows that the period has now doubled, as indicated in Fig. 5d. When the value of f is increased to 23, the response has a continuous, wide band power spectrum with some spikes on it, which confirms a chaotic motion of the system.

2.4 Bifurcation diagram

The bifurcation diagrams in Figs 6 and 7 show the long-term values of the angular displacement and angular velocity respectively, obtained by the fourth-order Runge–Kutta numerical integration algorithm, plotted against the dimensionless excitation amplitude $f \in [0, 30]$, in which the incremental value of f is 0.01. At each value of f the first 300 points of the Poincaré maps are discarded in order to exclude the transient state of motion. After that, the system is assumed to be in the steady state, the velocity for the next 200 points is plotted in the bifurcation diagram and only the stable limit set is plotted. The period doubling route to chaos is shown in the bifurcation diagram. The solution is a stationary point at the origin until $f = 4.14$ and supercritical bifurcation occurs. After this bifurcation, a period $1T$ attractor is generated. When f grows through 14.38, a symmetry-breaking bifurcation takes place and each period $1T$ orbit bifurcates into a period $2T$ attractor. When $f = 19.37$ a period $4T$ solution is generated. After that, there occurs a cascade of period doubling from $f = 19.37$ to 20.36, through which periods of the periodic motions become longer and longer: $T \times 2^n$ $(n = 0, 1, \ldots)$. When $f = 20.36$ the chaotic motion appears. It is noted that within the chaotic region there is a small interval in

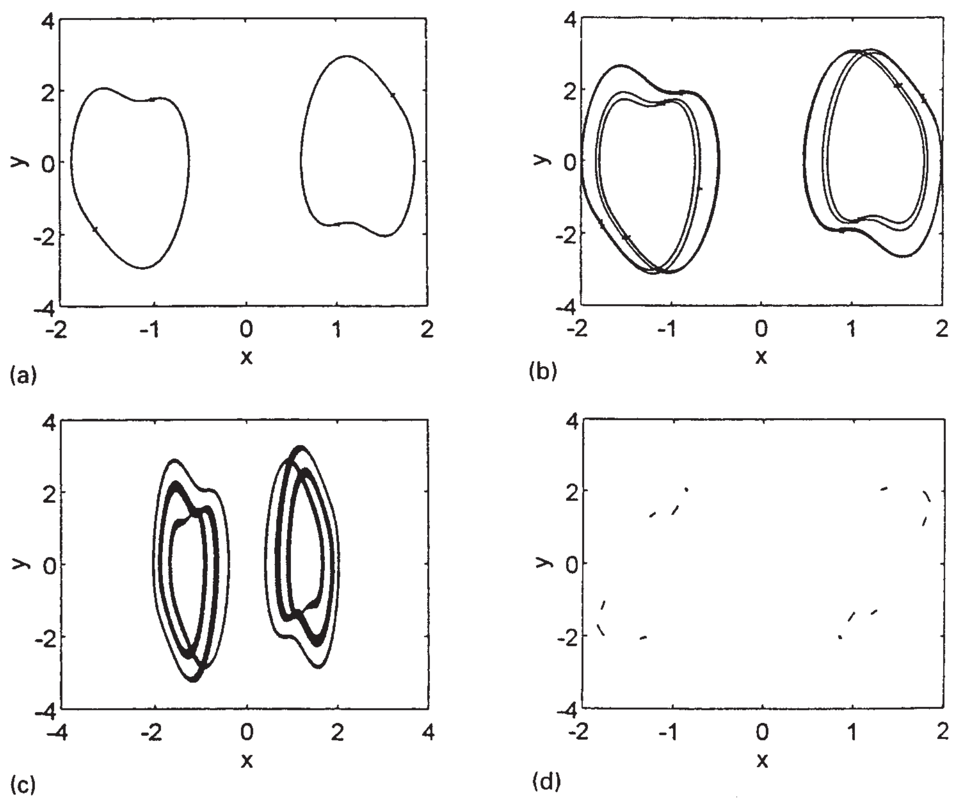

Fig. 4 (Continued over)

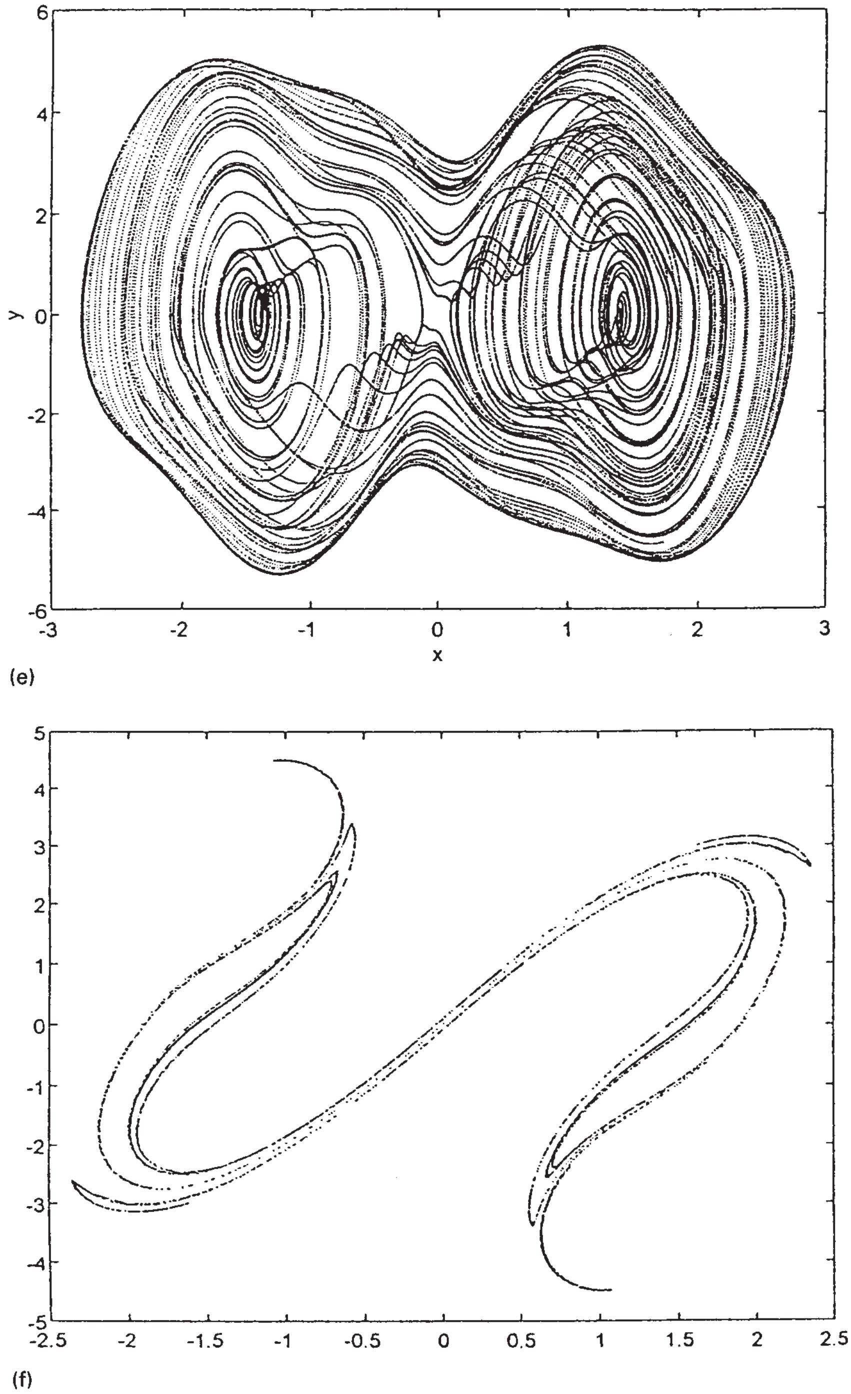

Fig. 4 Phase portraits and Poincaré points for (a) $f = 19$; (b) $f = 20.2$; (c), (d) $f = 20.37$; and (e), (f) $f = 23$

which the motion abruptly becomes periodic again. The sudden end of the chaotic attractor appears at $f = 25.95$.

2.5 Incremental harmonic balance method

The steady state periodic solutions of equation (3) can be obtained by the IHB method [**13**], which can deal with strong non-linearity very well and is convenient for computer implementation. Here the dimensionless time $\tau = \omega t$ is defined, $\bar{\varepsilon} = 0.5$ and $\beta = f/2$. Equation (3) then becomes

$$\omega^2 \ddot{x} + 2\alpha\omega\dot{x} + \gamma \sin x - \beta(1 - \cos \tau) \sin 2x = 0 \qquad (5)$$

where $(\cdot)$ represents a derivative with respect to the dimensionless time. The first step in this method is a Newton–Raphson procedure. Let $x_0(\tau)$ denote the current solution of equation (5) corresponding to the excitation parameters ω_0, γ_0 and β_0. A neighbouring

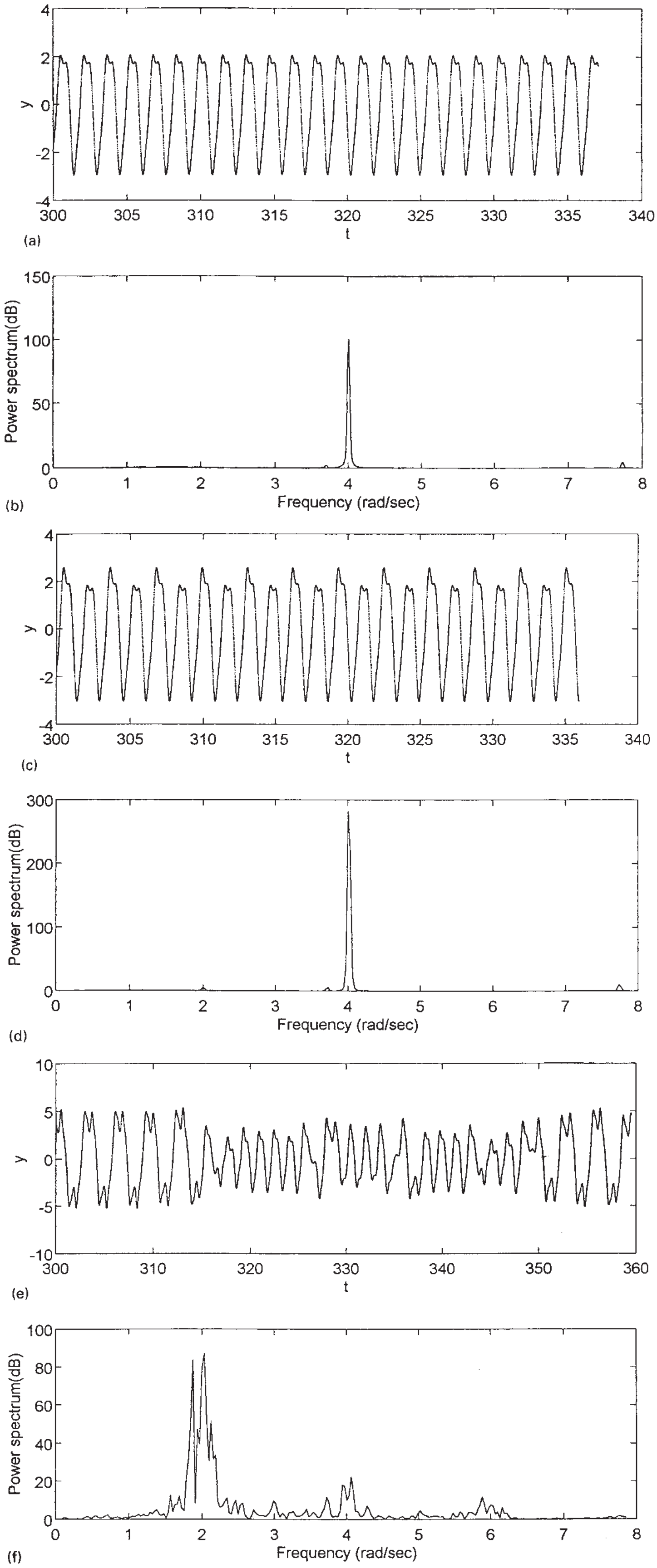

Fig. 5 Time history and power spectrum: (a), (b) period $2T$ motion for $f = 19$; (c), (d) period $4T$ motion for $f = 20$; (e), (f) chaotic motion for $f = 23$

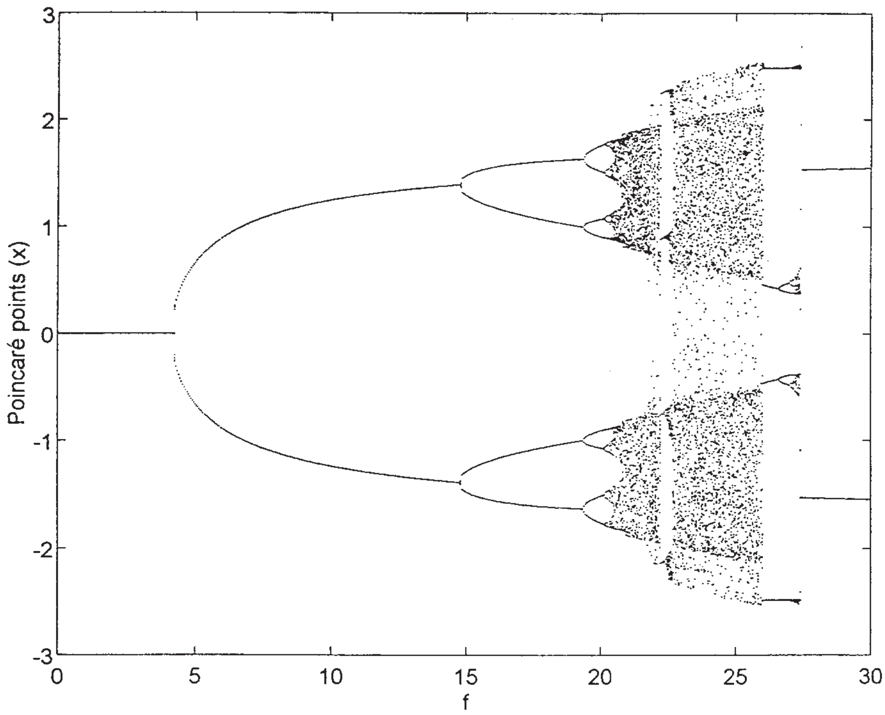

Fig. 6 Bifurcation diagram for the Poincaré points of angular displacement

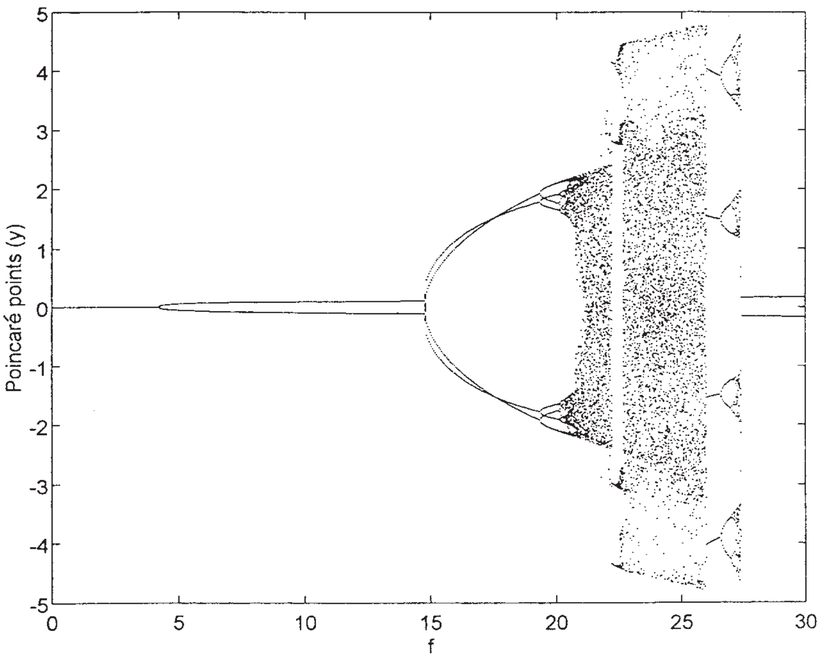

Fig. 7 Bifurcation diagram for the Poincaré points of angular velocity

solution is obtained by adding small increments to the current solution:

$$x = x_0 + \Delta x, \qquad \omega = \omega_0 + \Delta\omega$$
$$\gamma = \gamma_0 + \Delta\gamma, \qquad \beta = \beta_0 + \Delta\beta \tag{6}$$

For a small increment Δx, the non-linear terms $\sin x$ and $\sin 2x$ of equation (5) can be written as first-order Taylor expansions:

$$\sin x = \sin x_0 + \cos x_0 \Delta x$$
$$\sin 2x = \sin 2x_0 + 2\cos 2x_0 \Delta x \tag{7}$$

Substituting equations (6) and (7) in (5) and neglecting all the non-linear terms, the linearized incremental equation is obtained:

$$\omega_0^2 \Delta\ddot{x} + 2\alpha\omega_0\Delta\dot{x} + g_1(x_0, \tau)\Delta x = R + \Delta\omega F + \Delta\gamma P + \Delta\beta Q \tag{8}$$

where

$$g_1(x_0, \tau) = \gamma_0 \cos x_0 - 2\beta_0(1 - \cos\tau)\cos 2x_0 \tag{9}$$
$$R = -[\omega_0^2\ddot{x}_0 + 2\alpha\omega_0\dot{x} + g_2(x_0, \tau)] \tag{10}$$
$$g_2(x_0, \tau) = \gamma_0 \sin x_0 - \beta_0(1 - \cos\tau)\cos 2x_0 \tag{11}$$
$$F = -(2\omega_0\ddot{x}_0 + 2\alpha\dot{x}) \tag{12}$$
$$P = -\sin x_0 \tag{13}$$
$$Q = (1 - \cos\tau)\sin 2x_0 \tag{14}$$

The second step of the IHB method is the Galerkin procedure (see the Appendix).

From the Appendix, the qT period steady state solution $x_0(\tau)$ has been determined and its local stability is investigated by considering the following perturbed solution:

$$x = x_0 + \delta x \tag{15}$$

Inserting equation (15) into equation (5) and neglecting the terms of higher order in δx, the linear variational equation is obtained with periodic coefficients in the following form:

$$\omega^2\delta\ddot{x} + 2\alpha\omega\delta\dot{x} + g_1(x_0, \tau)\delta x = 0 \tag{16}$$

Equation (16) can be arranged in matrix form as

$$\dot{\mathbf{X}} = \mathbf{A}(\tau)\mathbf{X} \tag{17}$$

where

$$\mathbf{X} = [\delta\mathbf{x}, \delta\dot{\mathbf{x}}]^{\mathrm{T}}, \qquad \mathbf{A}(\tau) = \begin{bmatrix} 0 & 1 \\ A_{21} & -2\alpha/\omega \end{bmatrix}$$
$$A_{21} = -\frac{g_1(x_0, \tau)}{\omega^2} \tag{18}$$

Since x_0 is a periodic function of time τ with a period $T_q = 2q\pi$, the coefficient matrix $\mathbf{A}(\tau)$ has the same period T_q, i.e. $\mathbf{A}(\tau + T_q) = \mathbf{A}(\tau)$. The stability of a linear periodic system is analysed by the multivariable Floquet–Lyapunov theory with an efficient numerical scheme for computing the transition matrix at the end of one period, $\mathbf{\Phi}(T_q, 0)$. Here, the approximate transition matrix $\mathbf{\Phi}(T_q, 0)$ is given by the following:

$$\mathbf{\Phi}(T_q, 0) = \prod_{i=1}^{N_k}\left(\mathbf{I} + \sum_{j=1}^{N_j}\frac{(\Delta_i\mathbf{B}_i)^j}{j!}\right) \tag{19}$$

$$\mathbf{B}_k = \frac{1}{\Delta_k}\int_{\tau_{k-1}}^{\tau_k}\mathbf{A}(\xi)\,\mathrm{d}\xi \tag{20}$$

where N_k is the number of intervals in each period T; N_j is the number of terms in the approximation of the constant matrix $\mathbf{B}_i$ exponential; the kth interval is denoted by τ_k and its size by $\Delta_k = \tau_k - \tau_{k-1}$; in the kth interval the periodic coefficient matrix $\mathbf{A}(\tau)$ is replaced by a constant matrix $\mathbf{B}_k$.

The eigenvalues of the monodromy matrix $\mathbf{\Phi}(T_q, 0)$ are also called the Floquet multipliers (ρ_1, ρ_2) which can determine the stability of steady state solution. If all the modules of the eigenvalues ρ_k are smaller than unity, the solution is stable. If the module of one of the eigenvalues ρ_k is larger than unity, the solution is unstable. When an eigenvalue ρ_k passes through the unit circle, bifurcation occurs.

The solutions obtained by the IHB method in comparison with those obtained by numerical integration are shown in Figs 8a to c, in which the symbols $(\cdot)$ indicate the solutions obtained by the IHB method and the full curves indicate solutions obtained by numerical integration. These solutions agree well for the same parameters.

The different types of bifurcation can be verified by calculating the Floquet multipliers of the monodromy matrix as a function of parameter f as shown in Fig. 9. To investigate the bifurcation further, a Poincaré map is used to display the bifurcation diagram in Fig. 10, which shows the steady state Poincaré map.

3 GOVERNOR WITH AN ATTACHED COLLAR MASS *M*

The mass of the collar is neglected for simplicity in the previous investigation, and it can be seen from the above discussion that the simple model of the governor system exhibits complex non-linear and chaotic dynamics. A governor with an attached collar will now be studied.

3.1 Problem formulation

Using Lagrange's equation, the differential equation for the system is derived as follows:

$$(1 + 4\beta\sin^2\theta)\ddot{\theta} + 2\alpha\dot{\theta} + 2\beta\dot{\theta}^2\sin 2\theta + (1 + 2\beta)\gamma\sin\theta = \frac{1}{2}(f - 2\bar{\varepsilon}f\cos\omega t)\sin 2\theta \tag{21}$$

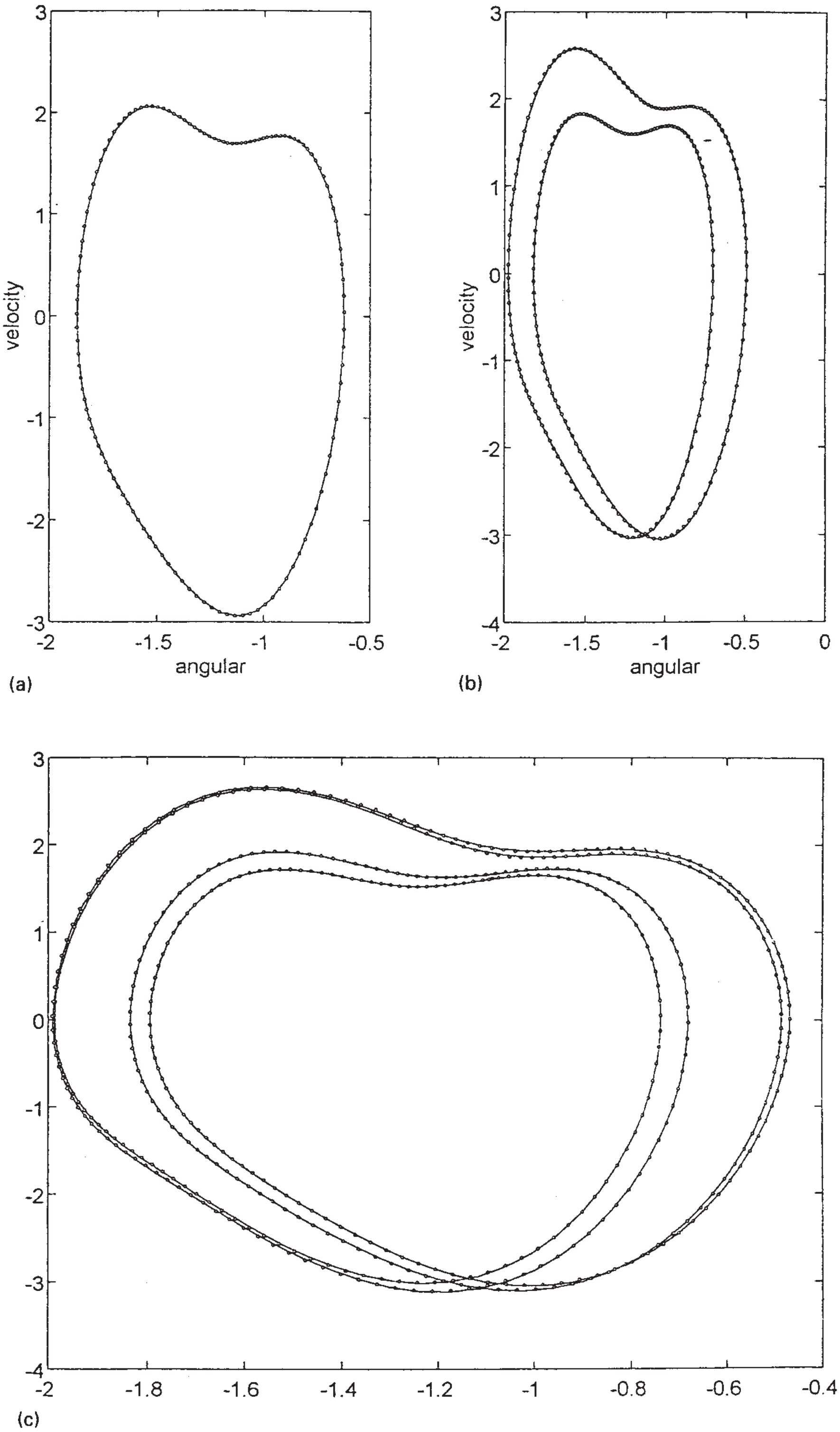

Fig. 8 Comparison between the IHB and numerical integration methods for (a) $f = 19$, (b) $f = 20$ and (c) $f = 20.2$

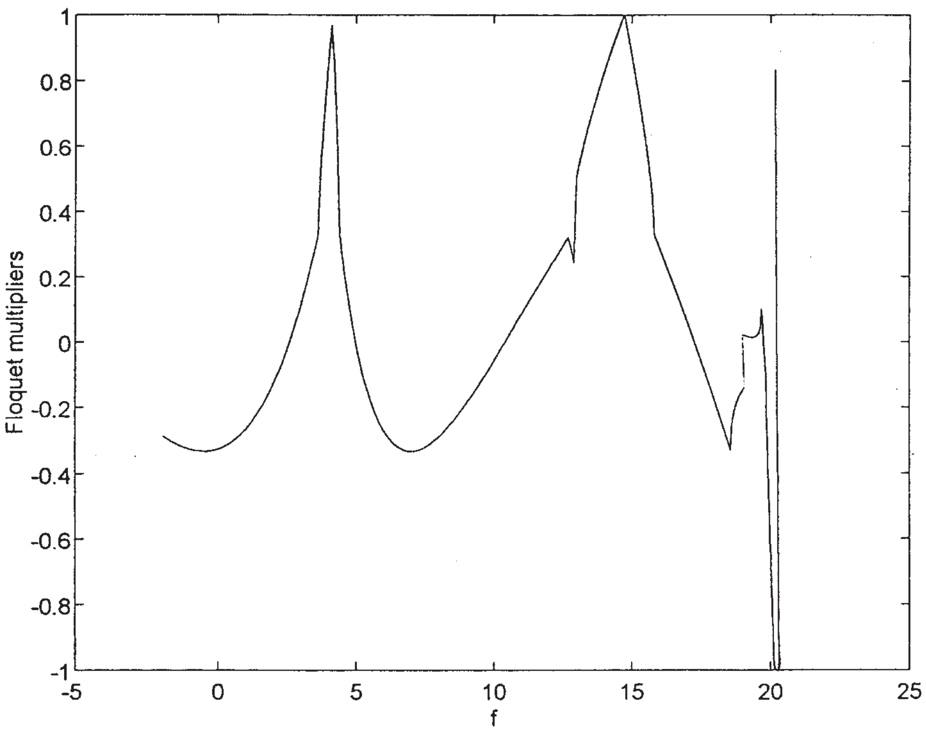

Fig. 9 Floquet multipliers as a function of f

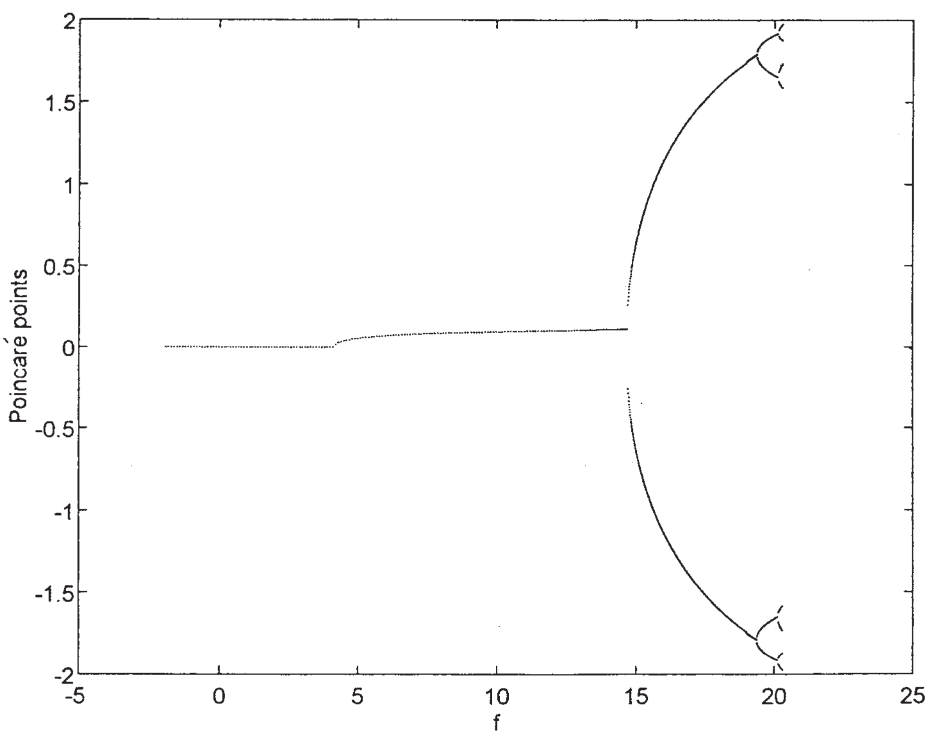

Fig. 10 Response in Poincaré section by the IHB method

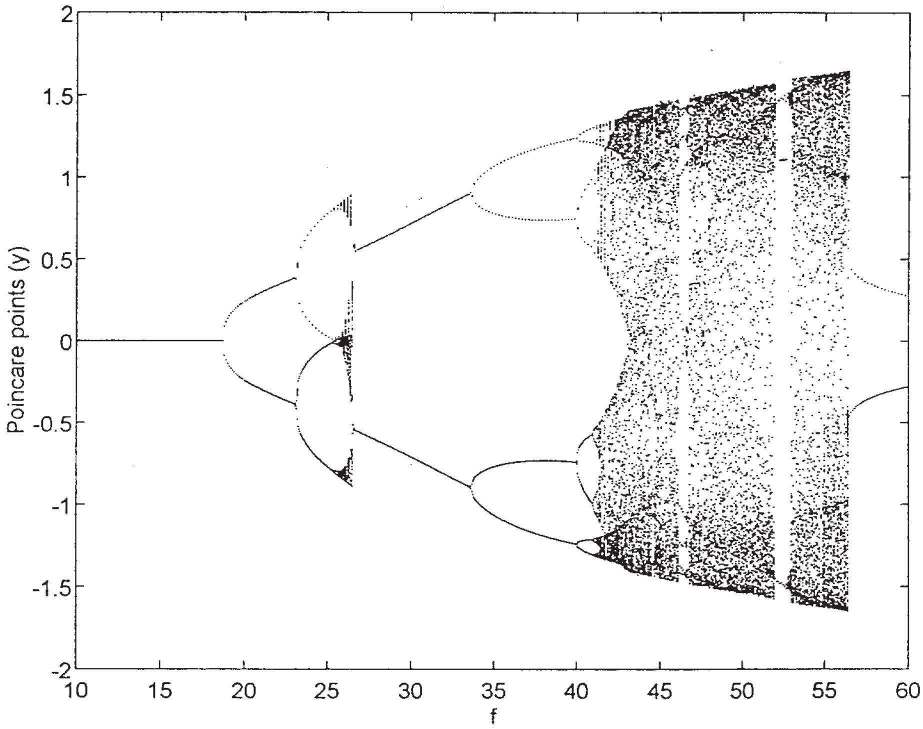

Fig. 11 Bifurcation diagram for $\bar{\varepsilon} = 0.3$ with 50 initial conditions

where $\beta = M/m$ (mass ratio), $2\alpha = c/m$, $\gamma = g/R$ and $f = \Omega_0^2$.

If $\tau = \omega t$, the dimensionless form of equation (21) is rewritten as

$$(1 + 4\beta \sin^2 \theta)\ddot{\theta} + 2\frac{\alpha}{\omega}\dot{\theta} + 2\beta\dot{\theta}^2 \sin 2\theta + \frac{(1+2\beta)\gamma}{\omega^2}\sin\theta = \frac{1}{2\omega^2}(f - 2\bar{\varepsilon} f \cos\tau)\sin 2\theta \tag{22}$$

With substitution of $\theta = x$, equation (22) becomes

$$(1 + 4\beta \sin^2 x)\ddot{x} + 2\frac{\alpha}{\omega}\dot{x} + 2\beta\dot{x}^2 \sin 2x + \frac{(1+2\beta)\gamma}{\omega^2}\sin x = \frac{1}{2\omega^2}(f - 2\bar{\varepsilon} f \cos\tau)\sin 2x \tag{23}$$

The number of the parameters affecting the system response is more than two. For example, let the rotational speed be the control parameter with the other parameters fixed. The transition from regular to chaotic motion is considered for the following values of the parameters of the system:

$$\beta = 0.2, \qquad \omega = 2, \qquad \frac{2\alpha}{\omega} = 1.2$$

$$\frac{(1+2\beta)\gamma}{\omega^2} = 4, \qquad \bar{\varepsilon} = 0.3$$

3.2 Numerical simulations and discussion

The bifurcation structure of the angular velocity component is shown in Fig. 11. The diagram shows a symmetry structure in which there are two chaotic regions. The solution is a stationary point at the origin until $f = 18.72$ and the system undergoes a supercritical bifurcation, whereupon a time periodic solution that is a period T Hopf bifurcation is generated. It is evident that, when f grows through 23.1, a symmetry-breaking pitchfork bifurcation takes place and each period $1T$ bifurcates into a subharmonic period $2T$. These motions then undergo a succession of complete period-doubling cascades (flip bifurcation), which eventually merge into the first chaotic region. The boundary crisis can be observed at $f = 26.58$, where it causes the chaotic attractor to be destroyed and results in a period $1T$ solution. It is clear that there are two narrow windows within the second chaotic region, one of which, period $5T$, exists between $f = 46.12$ and $f = 46.68$. Figure 12, which is an enlargement of the bifurcation diagram in Fig. 11 for f between 46.12 and 46.68, illustrates a period $5T$ window. For $f = 46.14$ a window of stable orbits appears.

4 GLOBAL ANALYSIS BY THE INTERPOLATED CELL MAPPING METHOD

In the study of non-linear dynamic systems the influence of initial conditions on system behaviour plays an

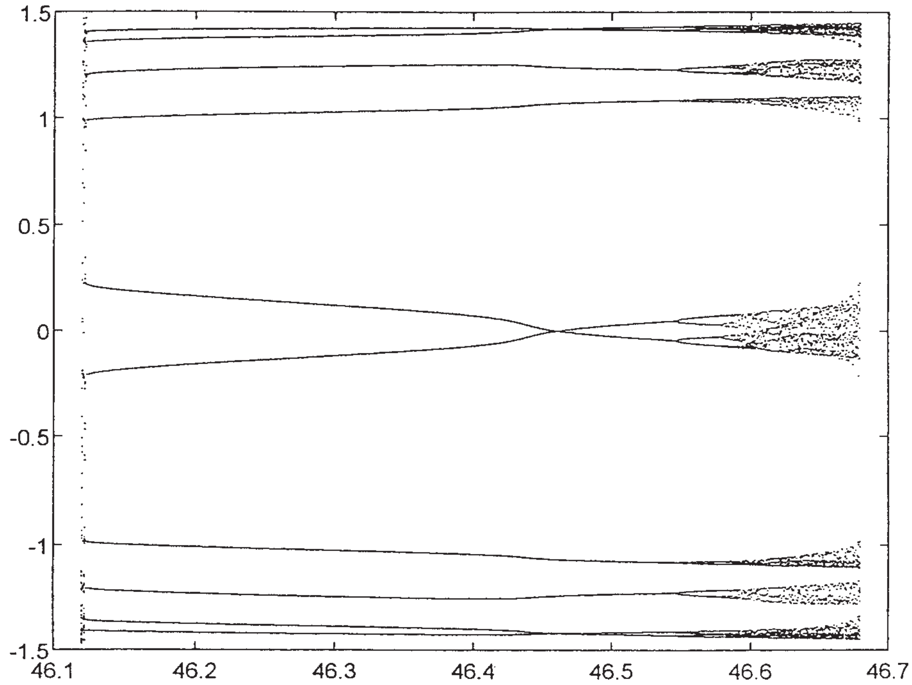

Fig. 12 Enlargement of the bifurcation diagram in Fig. 11, showing a period $5T$ window for $f = 46.12$–46.68

important role. For some system parameters, different initial conditions may lead to different attractors that may be regular or chaotic. Therefore, knowledge about attractors and the domains of attraction is very important when investigating a non-linear system. Attractors and domains of attraction must be delineated in the region of interest in order to characterize the global behaviour of a system.

Considering the case of $f = 18$, equation (4) becomes

$$\ddot{x} + 1.4\dot{x} + 4 \sin x = 9 \sin 2x - 9 \cos 8t \sin 2x \tag{24}$$

To apply the interpolated cell mapping algorithm, the first stage of any computation is to generate the mapping function from a 10 201 (101×101) grid of points distributed in the phase plane using a fourth-order Runge–Kutta integration algorithm. A trajectory is considered to be periodic when the distance between two trajectory states is less than 10^{-3}. When no periodic motion occurs until 20 interpolation steps, a trajectory is considered chaotic.

Figure 13 shows the result obtained by the ICM method applied to equation (24) for the region of interest: $-2.3 \leqslant x \leqslant 2.3$, $-2 \leqslant y \leqslant 2$. In Fig. 13 the domain of attraction of attractor 1 is depicted by dots, the domain of attraction of attractor 2 by the symbol $\times$ and the sink cell by the symbol $+$.

It is natural to study similar effects to the basin of attraction for the other parameters that control the system. In this problem, the effects of the damping term are considered. The values of the coefficient of damping are chosen as 2.0, 1.1 and 0.8 respectively in equation (24). Figures 14 to 16 show that different damping values can yield different attractors that correspond to

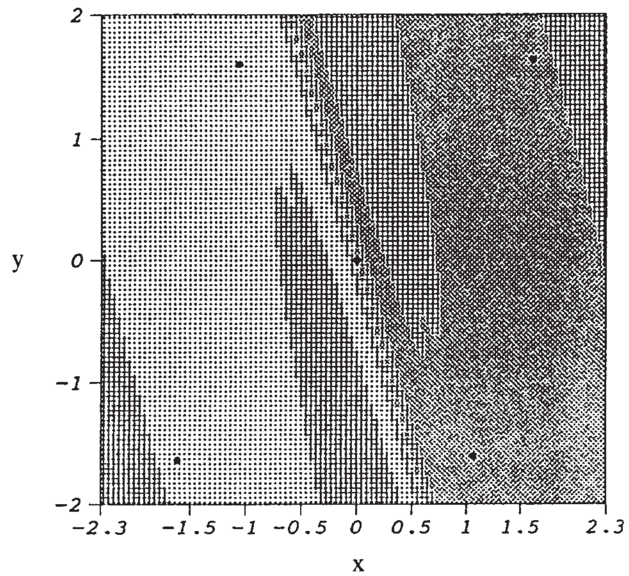

Fig. 13 Domains of attraction for period $2T$ motion of equation (24) with a damping value of 1.4

different multiperiodic solutions and cause different domains of attraction. In addition, the basins of attraction of the chaotic attractor when $f = 20.37$ and $f = 23$ in equation (4) are shown in Figs 17 and 18.

5 CONCLUSIONS

It has been shown that the simplified model of a fly-ball governor exhibits both regular and chaotic motions. Parametric studies have been performed by the IHB

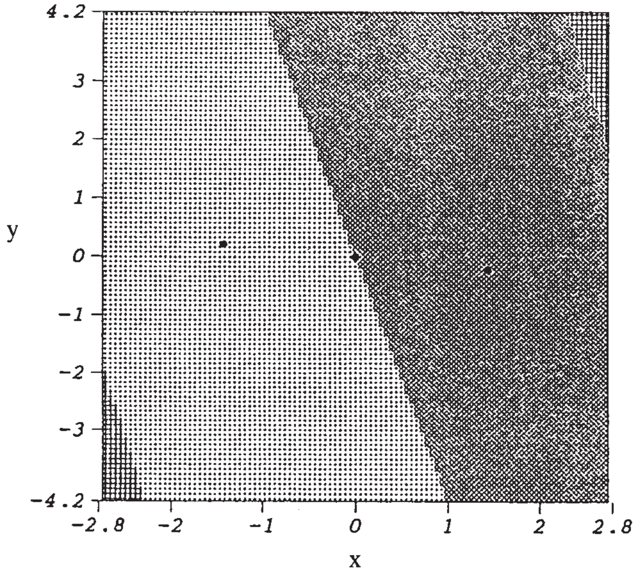

Fig. 14 Domains of attraction for period $1T$ motion of equation (24) with a damping value of 2.0

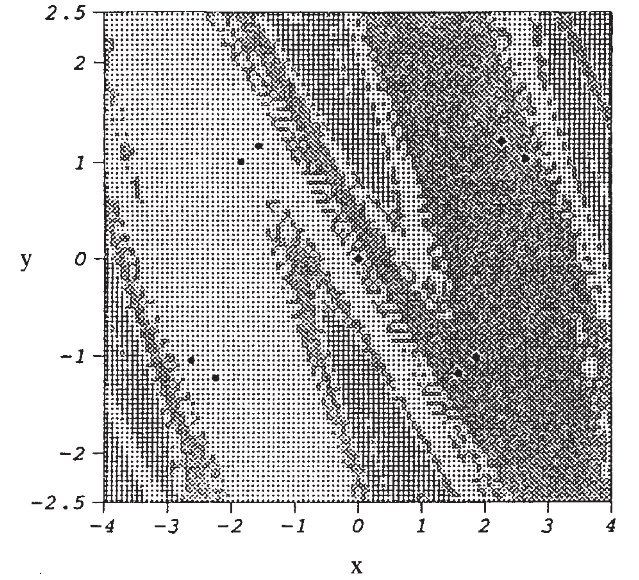

Fig. 15 Domains of attraction for period $4T$ motion of equation (24) with a damping value of 1.1

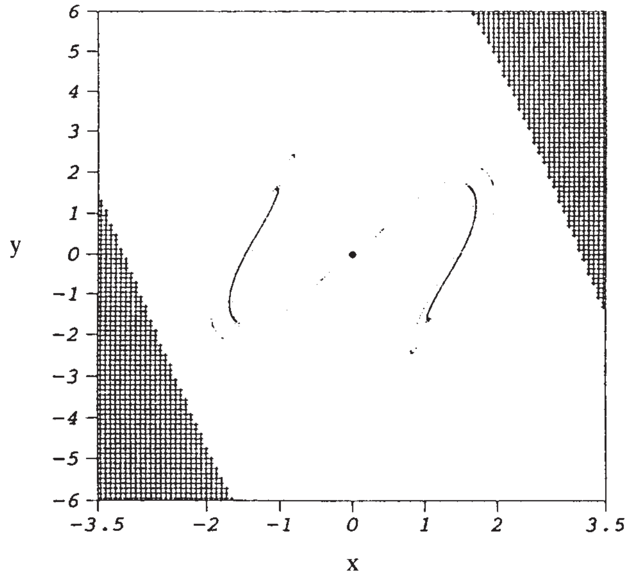

Fig. 16 Domains of attraction for chaotic motion of equation (24) with a damping value of 0.8

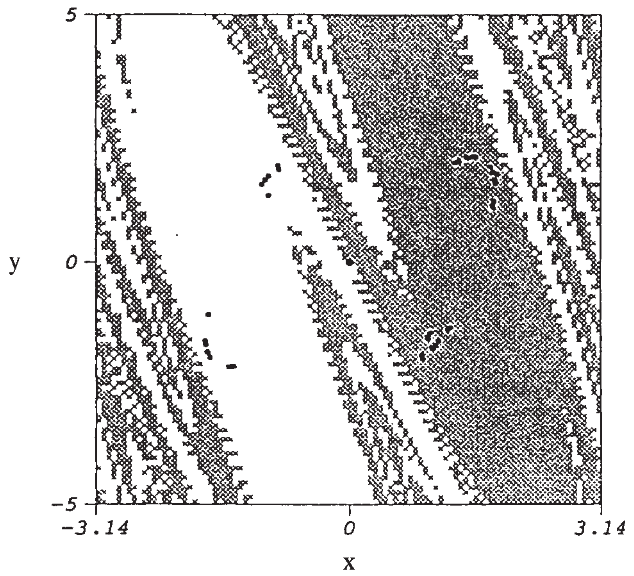

Fig. 17 Domains of attraction for chaotic motion of equation (24) with $f = 20.37$

method, the numerical integration method and other analytical techniques to analyse the behaviour of bifurcation and chaos. With the parametric studies the periodic solutions can be clearly guided by the IHB method and their stability is analysed by examining the movements of eigenvalues of the monodromy matrix. The solutions obtained by the IHB method are found to match exactly those obtained by numerical integration. A symmetry-breaking precursor to period-doubling bifurcation and a cascade of period doubling routes to chaos are observed in this system. Many of the characteristics available for detecting chaotic motion such as Lyapunov exponents, Lyapunov dimensions, Poincaré maps and power spectra are obtained numerically. Based on such analyses, many aspects of the dynamic behaviour of this simplified governor model are presented.

The global behaviour of the systems is obtained by means of the interpolated cell mapping method (ICM). The basins of attraction of the period attractor and chaotic attractor are obtained for certain system parameters of interest.

It must be emphasized that this mathematical model for a fly-ball governor is only a simplified one. The simplifications are not all reasonable, for instance the neglect of the $O(\bar{\varepsilon}^2)$ term in equation (4) for $\bar{\varepsilon} = 0.5$. The numerical data used are chosen to enrich the dynamic behaviour rather than to agree closely with the practical

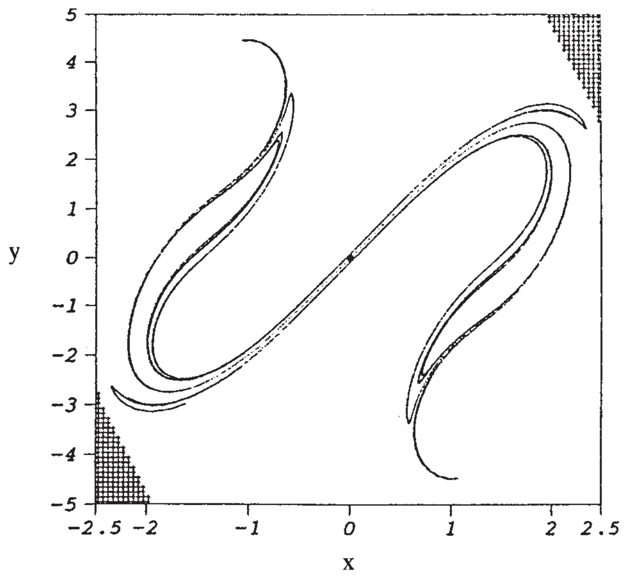

Fig. 18 Domains of attraction for chaotic motion of equation (24) with $f = 23$

data for actual governors. This paper serves as an introduction to the study of a more precise mathematical model of a fly-ball governor.

ACKNOWLEDGEMENT

This research was supported by the National Science Council, Republic of China, under Grant NSC87-2212-E-009-019.

REFERENCES

1. **Yagasaki, K., Sakata, M.** and **Kimura, K.** Dynamics of a weakly nonlinear system subjected to combined parametric and external excitation. *Trans. ASME, J. Appl. Mechanics*, 1990, **57**, 209.
2. **Sanchez, N. E.** and **Nayfeh, A. H.** Prediction of bifurcations in a parametrically excited Duffing oscillator. *Int. J. Non-Linear Mechanics*, 1990, **25**(2/3), 163.
3. **Szemplinska-Stupnicka, W., Plaut, R. H.** and **Hsieh, J.-C.** Period doubling and chaos in unsymmetric structures under parametric excitation. *Trans. ASME, J. Appl. Mechanics*, 1989, **56**, 947.
4. **Sekar, P.** and **Marayanan, S.** Periodic and chaotic motions of a square prism in cross-flow. *J. Sound Vibr.*, 1994, **170**(1), 1.
5. **Gottlieb, O.** Bifurcations and routes to chaos in wave-structure interaction systems. *J. Guidance, Control, and Dynamics*, 1992, **15**(4), 832.
6. **Ling, F. H.** and **Wu, X. X.** Fast Galerkin method and its application to determine periodic solution of non-linear oscillators. *Int. J. Non-Linear Mechanics*, 1987, **22**(2), 89.
7. **Lau, S. L.** and **Yuen, S. W.** The Holf bifurcation and limit cycle by the incremental harmonic balance method. *Computer Meth. Appl. Mech. Engng*, 1991, **91**, 1109.
8. **Friedmann, P., Hammond, C. E.** and **Woo, T. H.** Efficient numerical treatment of periodic systems with application to stability problems. *Int. J. Numer. Meth. Engng*, 1977, **11**, 1117.
9. **Tongue, B. H.** On the global analysis of nonlinear system through interpolated cell mapping. *Physica D*, 1987, **28**, 401.
10. **Tongue, B. H.** and **Gu, K.** Interpolated cell mapping of dynamical systems. *Trans. ASME, J. Appl. Mechanics*, 1988, **55**, 461.
11. **Wolf, A., Swift, J. B., Swinney, H. I.** and **Vastano, J. A.** Determining Lyapunov exponent from a time series. *Physica D*, 1985, **16**, 285.
12. **Baker, G. L.** and **Gollub, J. P.** *Chaotic Dynamics: an Introduction*, 1990 (Cambridge University Press).
13. **Cheung, Y. K., Chen, S. H.** and **Lau, S. L.** Application of the incremental harmonic balance method to cubic non-linearity systems. *J. Sound Vibr.*, 1990, **140**(2), 273.

APPENDIX

The approximate periodic solutions $x_0(\tau)$ and $\Delta x_0(\tau)$ for equation (8) may be expressed as

$$x_0 = \sum_{j=0,1,2,\ldots}^{N} \left(a_{j/q} \cos\frac{j}{q}\tau + b_{j/q} \sin\frac{j}{q}\tau \right)$$

$$\Delta x_0 = \sum_{j=0,1,2,\ldots}^{N} \left(\Delta a_{j/q} \cos\frac{j}{q}\tau + \Delta b_{j/q} \sin\frac{j}{q}\tau \right) \tag{25}$$

for unsymmetrical solution with period $2q\pi$ in terms of τ, and as

$$x_0 = \sum_{j=1,3,5,\ldots}^{2N-1} \left(a_{j/q} \cos\frac{j}{q}\tau + b_{j/q} \sin\frac{j}{q}\tau \right)$$

$$\Delta x_0 = \sum_{j=1,3,5,\ldots}^{2N-1} \left(\Delta a_{j/q} \cos\frac{j}{q}\tau + \Delta b_{j/q} \sin\frac{j}{q}\tau \right) \tag{26}$$

for symmetrical solution with period $2q\pi$ in terms of τ; N is the order of the harmonic to be taken into account and q is the order of the subharmonic. By applying the Galerkin procedure with Δa_k and Δb_k as the generalized coordinates, the following is obtained:

$$\int_0^{2q\pi} \{\omega_0^2 \Delta\ddot{x} + 2\alpha\omega_0\Delta\dot{x} + [1 + g_1(x_0, \tau)]\Delta x\}\delta(\Delta x)\,\mathrm{d}\tau$$

$$= \int_0^{2q\pi} (R + \Delta\omega F + \Delta\gamma P + \Delta\beta Q)\delta(\Delta x)\,\mathrm{d}\tau \tag{27}$$

Substituting equation (25) [or equation (26)] in equation (27) and matching the Δa_k and Δb_k terms, an incremental system of $2N+1$ (or $2N$) linear equations in terms of Δa_k and Δb_k is obtained in the form

$$\mathbf{C}\Delta a = \mathbf{R} + \Delta\omega\mathbf{F} + \Delta\gamma\mathbf{P} + \Delta\beta\mathbf{Q} \tag{28}$$

where

$$\mathbf{a} = [a_{j/q}, b_{j/q}]^{\mathrm{T}}$$
$$\Delta\mathbf{a} = [\Delta a_{j/q}, \Delta b_{j/q}]^{\mathrm{T}}$$
$$j = \begin{cases} 0, 1, 2, \ldots, N & \text{for symmetric solution} \\ 1, 3, \ldots, 2N-1 & \text{for unsymmetric solution} \end{cases} \tag{29}$$

$$\mathbf{C} = \begin{bmatrix} [C_1]_{ij} & [C_{12}]_{ij} \\ [C_{21}]_{ij} & [C_2]_{ij} \end{bmatrix}, \qquad \mathbf{R} = \begin{bmatrix} R_{1i} \\ R_{2i} \end{bmatrix}$$
$$\mathbf{F} = \begin{bmatrix} F_{1i} \\ F_{2i} \end{bmatrix}, \qquad \mathbf{P} = \begin{bmatrix} P_{1i} \\ P_{2i} \end{bmatrix}, \qquad \mathbf{Q} = \begin{bmatrix} Q_{1i} \\ Q_{2i} \end{bmatrix} \tag{30}$$

The expressions for **C**, **R**, **F**, **P** and **Q** are as follows:

Elements of matrix **C**:

$$[C_1]_{ij} = \mu_j \delta_{ij}\, q\pi \left[-\left(\frac{j\omega_0}{q}\right)^2 \right] + [C_1]_{ij}^{NL} \qquad (i, j = 0, 1, \ldots, N)$$

$$[C_{12}]_{ij} = 2\delta_{ij}\, q\pi \left(\frac{j\omega_0}{q}\right) + [C_{12}]_{ij}^{NL} \qquad (i = 0, 1, \ldots, N,\ j = 1, \ldots, N)$$

$$[C_{21}]_{ij} = -2\delta_{ij} q\pi \left(\frac{j\omega_0}{q}\right) + [C_{21}]_{ij}^{NL} \qquad (i = 1, \ldots, N,\ j = 0, 1, \ldots, N)$$

$$[C_2]_{ij} = \delta_{ij}\, q\pi \left[-\left(\frac{j\omega_0}{q}\right)^2 \right] + [C_2]_{ij}^{NL} \qquad (i, j = 1, \ldots, N)$$

where

$$\mu_j = \begin{cases} 2 & \text{for } j = 0 \\ 1 & \text{for } j \neq 0 \end{cases}, \qquad \delta_{ij} = \begin{cases} 1 & \text{for } j = j \\ 0 & \text{for } i \neq j \end{cases}$$

$$[C_1]_{ij}^{NL} = \int_0^{2q\pi} g_1(x_0, \tau) \cos\frac{i\tau}{q} \cos\frac{j\tau}{q}\, \mathrm{d}\tau$$

$$[C_{12}]_{ij}^{NL} = \int_0^{2q\pi} g_1(x_0, \tau) \cos\frac{i\tau}{q} \sin\frac{j\tau}{q}\, \mathrm{d}\tau$$

$$[C_{21}]_{ij}^{NL} = \int_0^{2q\pi} g_1(x_0, \tau) \sin\frac{i\tau}{q} \cos\frac{j\tau}{q}\, \mathrm{d}\tau$$

$$[C_2]_{ij}^{NL} = \int_0^{2q\pi} g_1(x_0, \tau) \sin\frac{i\tau}{q} \sin\frac{j\tau}{q}\, \mathrm{d}\tau$$

Elements of matrices **R**, **F**, **P** and **Q**:

$$R_{1i} = -\mu \left[-\left(\frac{i\omega_0}{q}\right)^2 \right] a_i + 2\alpha \left(\frac{i\omega_0}{q} b_i\right) q\pi + R_{1i}^{NL} \qquad i = 0, 1, \ldots, N$$

$$R_{2i} = -\left[-\left(\frac{i\omega_0}{q}\right)^2 \right] b_i - 2\alpha \left(\frac{i\omega_0}{q} a_i\right) q\pi + R_{2i}^{NL} \qquad i = 1, 2, \ldots, N$$

$$F_{1i} = 2q\pi\mu_i \left[\omega_0 \left(\frac{i}{q}\right)^2 a_i - \alpha \frac{i}{q} b_i \right], \qquad i = 0, 1, \ldots, N$$

$$F_{2i} = 2q\pi \left[\omega_0 \left(\frac{i}{q}\right)^2 b_i - \alpha \frac{i}{q} a_i \right], \qquad i = 1, 2, \ldots, N$$

$$\begin{Bmatrix} P_{1i} \\ P_{2i} \end{Bmatrix} = \int_0^{2q\pi} -\sin x_0 \begin{Bmatrix} \cos\dfrac{i\pi}{q} \\ \sin\dfrac{i\pi}{q} \end{Bmatrix} \mathrm{d}\tau$$

$$\begin{Bmatrix} Q_{1i} \\ Q_{2i} \end{Bmatrix} = \int_0^{2q\pi} (1 - \cos\tau) \sin 2x_0 \begin{Bmatrix} \cos\dfrac{i\pi}{q} \\ \sin\dfrac{i\pi}{q} \end{Bmatrix} \mathrm{d}\tau$$

where

$$R_{1i}^{NL} = -\int_0^{2q\pi} g_2(x_0, \tau) \cos\frac{i\tau}{q}\, \mathrm{d}\tau$$

$$R_{2i}^{NL} = -\int_0^{2q\pi} g_2(x_0, \tau) \sin\frac{i\tau}{q}\, \mathrm{d}\tau$$